Pressure induced synthesis and properties of an H_2S-H_2Se-H_2 molecular alloy

Miriam Peña-Alvarez,[†] Huixin Hu,[‡] Miriam Marqués,[†] Peter Cooke,[†] Mary-Ellen Donnelly,[‡] Jack Binns,[‡] Federico A. Gorelli,[‡] Eugene Gregoryanz,[‡,†] Philip Dalladay-Simpson,[*,‡] Graeme J. Ackland,[†] and Ross T. Howie[*,‡]

†*Centre for Science at Extreme Conditions and School of Physics and Astronomy, University of Edinburgh, Edinburgh EH9 3FD, United Kingdom*

‡*Center for High Pressure Science Technology Advanced Research (HPSTAR), Shanghai*

E-mail: philip.dalladay-simpson@hpstar.ac.cn; ross.howie@hpstar.ac.cn

Abstract

The chalcogens are known to react with one another to form interchalcogens, which exhibit a diverse range of bonding and conductive behaviour due to the difference in electronegativity between the group members. However, the interchangeability between sulfur and selenium atoms in molecular chalcogenides, to form mixed chalcogenide hydrides has not yet been experimentally explored. Through a series of high pressure diamond anvil experiments combined with density functional theory calculations, we report the synthesis of an S-Se hydride. At pressures above 4 GPa we observe the formation of a single solid comprised of both H_2Se and H_2S molecular units. Further compression in a hydrogen medium, leads to the formation of an alloyed compound $(H_2S_xSe_{1-x})_2H_2$, after which there is a sequence of pressure-induced phase transitions associated with the arrested rotation of molecules. The formation of the alloy stabilizes the H_2Se molecule to higher pressures than observed in the pure system. At pressures

above 50 GPa, there is a symmetrisation of hydrogen bonds concomitantly with the closing band gap and increased reflectivity of the compound, indicative of a transition to a metallic state. The existence of the molecular alloy opens the possibility to tune electronic properties by varying the S/Se concentration.

The report of high temperature superconductivity at 190 K and 200 GPa in hydrogen sulfide (H_3S) was a defining moment in the research of dense hydrogen-rich systems.[1] As such, the H-S system has been comprehensively investigated, with the majority of studies investigating the synthesis pathway of H_3S from either an H_2S precursor, or by laser heating S+H_2.[1–3] It is still of great intrigue of how the low pressure insulators, H_2S, and the van der Waals compound, $(H_2S)_2H_2$, transforms to metallic H_3S at high densities.[1–5]

At low pressures $(H_2S)_2H_2$ adopts phase I with a Al_2Cu type $I4/mcm$ structure with H_2 molecules hosted within channels formed by an H_2S framework.[4,5] On further compression above 16 GPa, changes in the vibrational Raman spectra were attributed to a transition to a second phase, phase II (and II'), before transforming to phase III in which the S atomic configuration is better described by $Cccm$ symmetry. At higher pressure, there is a predicted transition from $Cccm$ to non-molecular $Im\bar{3}m$ which is metallic and superconducting with T_c values of 191 to 204 K at 200 GPa.[2] Although superconductivity in H_2Se and H_2Te[6] has been predicted in both systems, experimental results suggest that neither is stable at the theoretically estimated conditions for superconductivity.[7,8]

It is well known that in transition metal chalcogenides the electronic band gap can be modified by the substitution of S by Se.[9–11] Following this approach, recent studies have explored hypothetical Se doping in the superconducting $Im\bar{3}m$ H_3S system.[12–14] Liu *et al.*[13] found that $S_{0.5}Se_{0.5}H_3$ would prefer an ordered structure over structural disorder, but the Se-doping would reduce the T_c.[13] Amsler[14] broadened the composition range of S/Se within the (S,Se)H_3 $Im\bar{3}m$ structure, finding a variety of stable compositions above 150GPa, again with T_c lower that in the pure sulfur system: this was associated with the reduced strength of the covalent bonding in these metallic systems.[12–14]

Theoretical investigations of Se-doping have only explored the metallic $Im\bar{3}m$ H_3S, and did not account for any $(H_2S)_2H_2$ molecular phases.[12–14] The $(H_2S)_2H_2$ material is formed by H_2S and H_2 molecular units held by hydrogen bonding and van der Waals interactions. Therefore, theoretical studies on Se substitution of $(H_2S)_2H_2$ remain uncharted territory.

By combining SeS_2 (or S + Se) with excess H_2 in a diamond anvil cell (DAC) we synthesize a molecular alloy $(H_2S_xSe_{1-x})_2H_2$ above 4.5 GPa. Density functional theory calculations predict that the alloy has substitutional disorder at room temperature, with any stoichiometry being possible. Comparing molecular dynamics (MD) calculations with Raman spectroscopic and x-ray diffraction experiments, we identify that phase I adopts $I4/mcm$ symmetry with rotating molecules before transforming to $I422$ symmetry (phase II), and subsequently to $Cccm$ (phase III) where molecular rotation stops. The vibrational Raman spectra disappears in phase III, indicative of hydrogen bond symmetrisation, whilst we observe band gap closure and increased reflectivity suggestive that the sample is metallic above 55 GPa.

We have investigated two synthesis pathways; SeS_2+H_2 and S+Se+H_2, with the ratio of S:Se approximately 1:1. All samples were loaded with an excess of H_2 at 0.2 GPa (See SI for experimental details). After loading, the pressure was increased to 0.5 GPa, and the sample heated to 473 K. At this temperature, the SeS_2 (or S + Se) precursor was observed to react immediately with the surrounding H_2. On temperature quench, Raman spectroscopy measurements confirmed the synthesis of a fluid mixture of H_2S, H_2Se and H_2 through their corresponding intramolecular vibrational excitations (vibrons).

Between pressures of 0.5 GPa and 1 GPa, we observed the formation of crystals (see Fig. S1) that exhibit both H_2S and H_2Se vibrational excitations (Fig. S2). Each crystal in a given sample showed uniform intensity of the H_2S:H_2Se vibrational modes, alluding to the formation of an interchalcogen molecular alloy, $H_2S_xSe_{1-x}$. X-ray diffraction patterns were consistent with the formation of single crystals indexed to $Fm\bar{3}m$ (a=5.3362(4) Å) equivalent to phase I of H_2S/H_2Se with unit cell volumes at intermediate values (Fig. S3).

Upon further compression above 4.5 GPa, the crystals visibly changed shape (see pho-

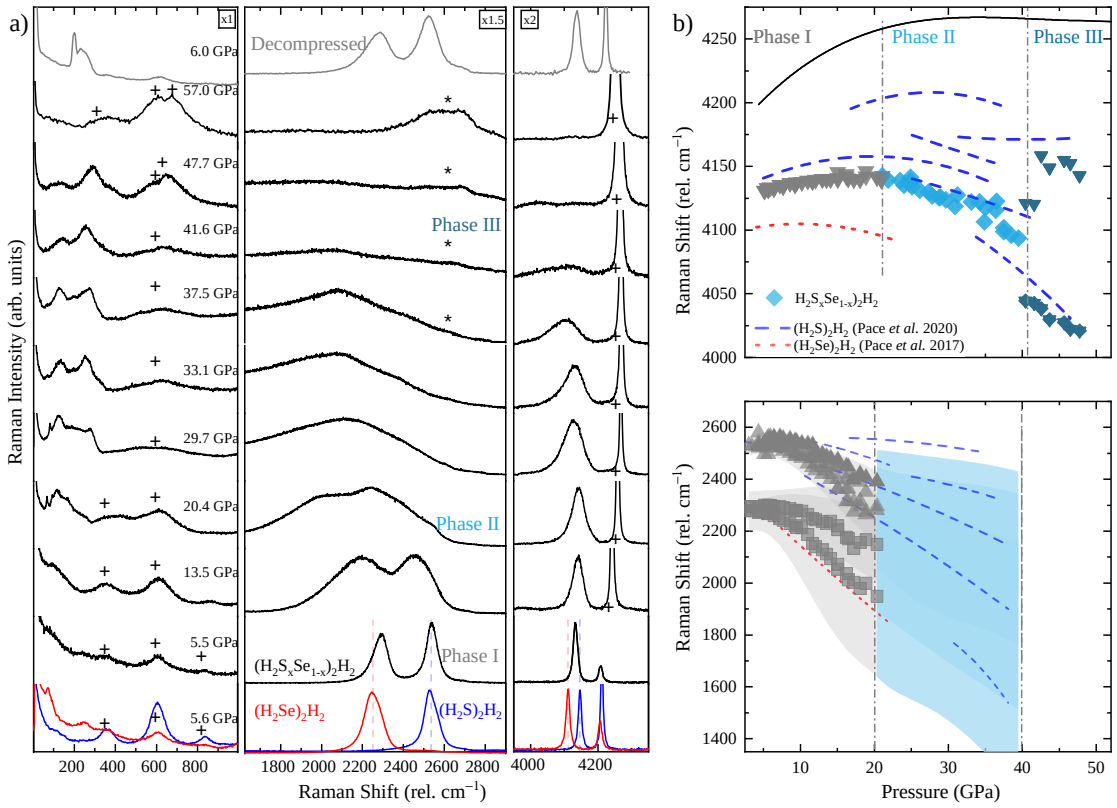

Figure 1: a) Representative Raman spectra on compression of $(H_2S_xSe_{1-x})_2H_2$ at 300 K. For comparison, the spectra of $(H_2S)_2H_2$ (blue) and$(H_2Se)_2H_2$ (red) at 5.6 GPa are shown.[4,5,7] The top spectrum is measured on decompression after a pressure cycle to 57 GPa, demonstrating the reversibility of the phase transitions. The H_2 modes (rotons, phonon and vibron) originating from excess H_2 are indicated by a cross, while the second order Raman of diamond is indicated by an asterisk. b) Raman shift as a function of pressure for the $(H_2S_xSe_{1-x})_2H_2$ compound. Top panel: The H_2 vibron frequencies as function of pressure. Filled symbols and crosses correspond to Raman and IR measurements respectively. Bottom panel: The frequencies of the H-S and H-Se stretching bands are shown by symbols in phase I. Above 20 GPa the individual components are indistinguishable and represented by a shaded region reflecting the full width at half maximum of the band. Blue and red dashed lines in both panels correspond to data of $(H_2S)_2H_2$ and $(H_2Se)_2H_2$, respectively.[5,7] Vertical dotted-dashed lines indicate the phase I, II and III transition pressures.

tomicrographs in Figs. 2 and S1) and a new vibrational Raman mode appears at 4129 cm^{-1} (Fig. 1). This new mode, which we denote ν_1-H_2 is lower than the frequency of the surrounding H_2 media, and corresponds to H_2 units in a new compound, which we identify as $(H_2S_xSe_{1-x})_2H_2$. Comparison of the spectral features between $(H_2S_xSe_{1-x})_2H_2$ with those of the binary systems, $(H_2S)_2H_2$ and $(H_2Se)_2H_2$, at similar pressures indicates that an analo-

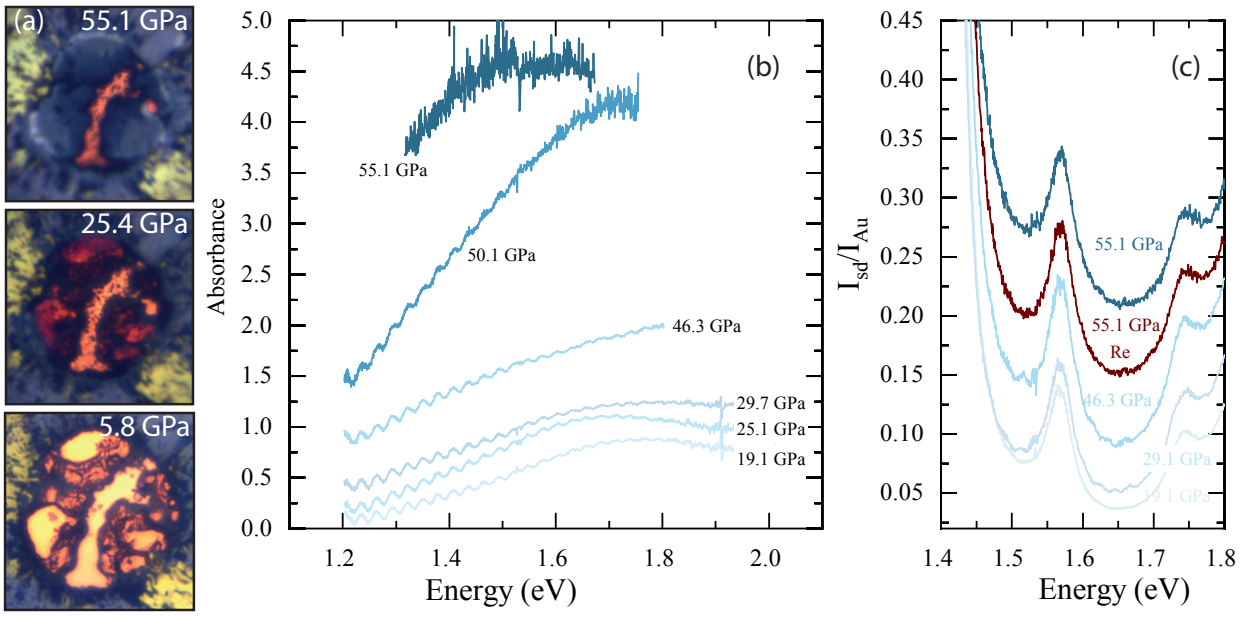

Figure 2: a) Photomicrographs of the sample in phase I (5.8 GPa), phase II (25.4 GPa) and phase III (55.1 GPa). Gold foil can be observed on the gasket which is used as a reference for reflectivity measurements. At 55.1 GPa, the transmitted light from the sample is from unreacted H_2. b) Representative absorption spectra on compression from a supercontinuum source. At 55.1 GPa, there is no transmitted light through the sample and the absorption is identical to the background spectrum. c) Representative reflectivity data from a supercontinuum source at various pressures relative to a gold reference, where I_{sd} is the sample-diamond interface and I_{au} is the gold-diamond interface. Reflectivity markedly increases with pressure in phase III and at 55.1 GPa has a higher reflectivity compared with the rhenium gasket (red spectrum).

gous structure has formed (Fig. 1 & S4-5.)[4,5,7] On decompression, we find $(H_2S_xSe_{1-x})_2H_2$ stable to at least 1 GPa, below which the sample transforms back to a mixed fluid.

Fig. 1a shows the Raman spectra of $(H_2S)_2H_2$ and $(H_2Se)_2H_2$ at 5.6 GPa, where their two most characteristic features are the H_2S and H_2Se band centred at 2537 and 2257 cm^{-1}, respectively; and the ν_1-H_2 mode at 4145 and 4110 cm^{-1}, respectively. Comparing with our experimental results for $(H_2S_xSe_{1-x})_2H_2$ (see Fig. 1), we find that the ν_1-H_2 is shifted to an intermediate value (4125 cm^{-1} at 5.6 GPa) between that of $(H_2S)_2H_2$ and $(H_2Se)_2H_2$. At this pressure, the widths of the vibrons in both the binary and the ternary compound are comparable.

X-ray diffraction patterns are consistent with those observed for phase-I of the binary

compounds $(H_2S)_2H_2$ and $(H_2Se)_2H_2$.[4,5,7] At 4.75 GPa the refined unit cells parameters indexed in *I4/mcm* were a = 7.4087(2) Å, c = 6.1222(1) Å, and volume of 336.04(1) Å^3 (see Fig. 3). This volume lies between the values observed for the binary host-guest compounds, evidence that the product is a ternary molecular alloy rather than a mixture of two binary compounds. If a mixture was formed, one would expect to see splitting of all the diffraction peaks, which is not observed here. Due to poor powder quality, a full Rietveld refinement was not possible, however a comparison of Le bail refinements is shown in Fig. S6 between the unit cell described above and S/Se atoms in the 8h position (x=0.34047, y =0.15953) with occupancies of 0.5.

To further investigate the arrangement of sulfur and selenium atoms, we have calculated the formation enthalpies for various ordered supercells as implemented in the ATAT and VASP codes[15,16] performed on $I4/mcm$ at 5 GPa (see Fig. 3c). At 0 K the $I4/mcm$ structure is clearly unstable versus distortions of the hydrogen arrangements for pure $(H_2S)_2H_2$ and $(H_2Se)_2H_2$ and mixed S/Se ratios. Therefore, we allowed it to distort and considered the resulting low-symmetry structure ($P1$) as the reference structure for the cluster expansion (CE). The associated enthalpies of the most stable structures are higher than for decomposition into the pure compounds in $P1$, but typically only by about 2meV. This allows the possibility of an S/Se order-disorder transition. We have also considered the $I4/mcm$ structure proposed by Strobel,[4] the $C2/c$ structure predicted to be stable at 0 K for $(H_2S)_2H_2$[17] and a low symmetry structure $I422$ found in the convex hull at x=0.5 when the end pure species have $I4/mcm$ symmetry.

To investigate the order-disorder transition, we use a Monte Carlo approach,[18,19] treating Se and S as Ising spins with neighbours determined from the DFT structure (See SI for further information). The order-disorder transition in this system can be identified from a sharp peak in the heat capacity (Fig. S7).[18,19] In reduced units the transition occurs T=3 for the alloying system, or T=8.5 for the demixing case where there are no stable compound phases on the convex hull. To convert this to an estimate of the transition temperature,

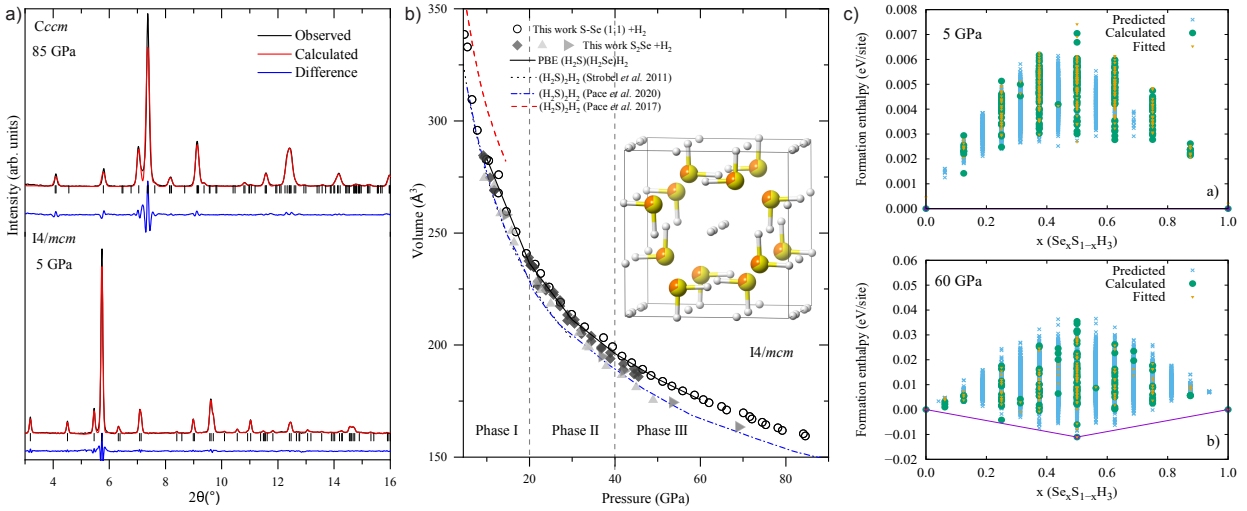

Figure 3: (a) Le Bail refinement fit of the $I4/mcm$ and $Cccm$ structures for $(H_2S_xSe_{1-x})_2H_2$ to x-ray diffraction ($\lambda = 0.2922$ Å) data collected at 5 GPa (lower) and at 85 GPa (upper). b)Refined unit cell volumes as a function of pressure compared to volumetric data from $(H_2S)_2H_2$, $(H_2Se)_2H_2$.[4,5,7] c) Formation enthalpies for $Se_xS_{1-x}H_3$ from a cluster expansion performed with ATAT at 5 GPa (top) and 60 GPa (bottom). At 5 GPa the end points are the binary phases $(H_2S)_2H_2$ and $(H_2Se)_2H_2$ in a structure derived from the $I4/mcm$ symmetry after allowing distortion.[4] At 60 GPa the $Cccm$ structure is taken as starting point. The green solid circles correspond to enthalpies of structures calculated with VASP. The triangles denote the fitted enthalpies from the CE and the crosses denote enthalpies of predicted structures

the units are fitted to the DFT data (Fig 3c) where we see that the formation enthalpy of a disordered structure is 5.5 meV/site (implying J_1 = 1meV/bond). This implies an order-disorder temperature of J_1 = 8.5 meV = 100 K. In Fig. 3(c) the energy differences are even smaller, therefore the stable compounds predicted will be disordered at even lower temperatures. Despite the approximations involved in this calculation, it is clear that the DFT energies imply a disordered alloy at room temperature.

On compression of $(H_2S_xSe_{1-x})_2H_2$ phase I, we observe an increase of the ν_1-H_2 vibron frequency, whilst the H-S and H-Se vibrational bands continually decrease in frequency. Between 15 - 20 GPa, we observe asymmetric broadening of the ν_1-H_2 Raman mode, together with a redistribution of intensity of the H-S and H-Se vibrational bands (see Fig.1). Simultaneously, we observe the emergence of distinct Raman lattice modes.

Similar changes were also observed at equivalent pressures in $(H_2S)_2H_2$, interpreted as a

transition to a phase II (and II'), however the vibrational spectra are more complex, with ν_1-H_2 splitting into 4 distinct modes by 25 GPa in the binary compound (see Fig.1 and Fig. S4 for comparison).[5] Conversely, no splitting of ν_1-H_2 was observed in the equivalent Se compound up to pressures of 22.5 GPa.[7] Interestingly, the ν_1-H_2 of the alloy more closely resembles $(H_2Se)_2H_2$, however we observe the H_2Se units are stabilized to considerably higher pressure in the alloy compared to the binary system, which decomposes above 22 GPa at 300 K.[7] Together with the spectral changes, we observe the sample becoming visibly red above 20 GPa, with absorption measurements indicating a rapidly closing band gap with pressure (Fig. 2).

Applying further pressure to the compound, we observe the H-S and H-Se bands in phase II of $(H_2S_xSe_{1-x})_2H_2$ continuously broaden and decrease in intensity with pressure. Above 40 GPa, the modes are indistinguishable from the background Raman signal, whilst simultaneously, the ν_1-H_2 mode is superseded by two distinct modes at 4040 and 4160 cm^{-1}. We attribute these changes as a transition from phase II-III, analogous to the H-S system. No detectable transmission in the visible is observed above 55 GPa, and the $(H_2S_xSe_{1-x})_2H_2$ crystals becomes indistinguishable from the gasket (Fig. 2a). Reflectivity in the visible significantly increases, with a reflectivity of 22% compared with the gold reference at 745 nm at 55.1 GPa and values higher than the rhenium gasket (Fig. 2c). The reflectivity values of the $(H_2S_xSe_{1-x})_2H_2$ sample is likely underestimated as the gold reference is bridged between the diamond and gasket, whilst the sample has varied topography. These combined measurements indicate that at these pressures the sample is transforming to a metallic state. We find the insulator-to-metal transition reversible on decompression (Fig. S1), together with the reversibility of the I-II-III phase sequence, ruling out sample decomposition.

X-ray diffraction measurements show no distinct changes in the S/Se positions up to pressures of approx. 85 GPa (Fig.3 and S7-8), above which the analysis of the diffraction pattern is more consistent with *Cccm* space group, with a = 8.1610(19), b = 8.217(2) and c = 4.7553(10) Å (see Fig. 3 and S6). It is worth noting that the $I4/mcm$ (tetragonal) and

$Cccm$ (orthorhombic) symmetries are indistinguishable if the unit cell dimensions a and b are identical.

DFT calculations for $(H_2Se)_2H_2$ at 0 K reveal a similar set of candidate structures to those predicted for $(H_2S)_2H_2$ (see Fig. S8).[2,17] All of these predicted phases, $P1$, $I4/mcm$, $I422$, and $Cccm$, cannot be distinguished on the basis of x-ray diffraction alone due to the low scattering efficiency of hydrogen.[2,4,5,7,8] Between 5 and 100 GPa the most stable 0 K structures with chalcogenide positions close to $I4/mcm$ have hydrogen positions breaking symmetry: to $P1$ at low pressure, with bond symmetrization increasing the symmetry to $Cccm$ around 30 GPa (Fig. S20-26). Static lattice stability of $Cccm$ over $C2/c$ occurs above 80 GPa (see Fig S16). We have calculated the formation enthalpies for various ordered supercells[15] performed on $Cccm$ at 60 GPa, Fig. 3(c) using ATAT+VASP codes. The convex hull demonstrates that at 60 GPa one structure is stable versus decomposition into the pure compounds, however at both 5 GPa and 60 GPa the energy differences between the most stable structures at different x are very small.

Our DFT-MD simulations indicate that above 20 GPa, the H_2S and H_2Se molecules are no longer rotating freely. $I422$ would present the same S/Se arrangements but has a lower symmetry than the initial $I4/mcm$, thus we consider this tentative symmetry as an intermediate between the $I4/mcm$ (phase I) and the $Cccm$ (phase III). The averaged S/Se atomic positions remain close to $I4/mcm$ which is consistent with our x-ray diffraction measurements. The H_2S and H_2Se molecules can be viewed as a hydrogen-bonded network with H_2 accommodated in two types of channel (see Fig. S9, S10 for structural representations and Fig. S11 for electron localization function (ELF) representation). In one channel the surrounding square of Se/S atoms is hydrogen-bonded, whilst in the other, the Se/S are directly adjacent. The H_2 molecules in the larger channels rotate in the xy plane, while in the narrower channels they are oriented along the z-axis.

The phase transitions are primarily driven by hydrogen-bonding, with changes in the H_2S/H_2Se molecules orientation and in the nature of the H_2 sites within the lattice (see

Fig. S12 for H-S/H-Se and H-H distances predicted for an alloy in compression). Therefore through Raman spectroscopy, we can compare the experimental Raman spectra with the unique spectral features of each candidate structure.[4,5,20,21] Fig. S14 shows the experimental Raman frequencies of the H-Se and H-S stretching modes compared with the those calculated for the $I4/mcm$, $I422$ and the $Cccm$ structures of the binary compounds, $(H_2S)_2H_2$ and $(H_2Se)_2H_2$.The calculated Raman for the low symmetry $I422$ shows significant splitting of the H-S and H-Se modes, agreeing with the experimentally observations in phase II. Although for disordered S/Se mixtures there are numerous components in each peak arising from the different local environments, we do observe a good agreement between the experimental results and the calculated Raman for the three phases of the pure species. Symmetry dictates that $I4/mcm$ has only a single Raman-active vibron, but DFPT calculations and DFT-MD simulations at 300 K for the $Cccm$ structure, suggest two ν-H_2 modes separated by 200 cm^{-1} (using 100% S or Se). This is in qualitative agreement with our experimental data for phase III (see Fig.S14 for the calculated vibrons for the $P1$ structure of Duan *et al.*[2])

The sequence of observed alloy phases can be deduced by a combination of Raman, x-ray and DFT, as summarized in Table 1. All three methods indicate that there is a continuous solid solution of $(H_2S_xSe_{1-x})_2H_2$. At low pressures (5 GPa) and room temperature, H_2, H_2Se and H_2S molecules are rotating freely and the high symmetry $I4/mcm$ structure with one H_2 vibron is generated. When increasing pressure (around 20 GPa), the rotation of the H_2(S,Se) molecules is hindered due to an increase of the strength of the hydrogen bonding. This symmetry decrease splits the H-Se and H-S vibrons. Splitting of the H_2 vibrons, which becomes even clearer in phase III, can be associated to an xy-rotor and a z-libron in the two different hydrogen channels. Interestingly, the H_2Se molecule is stabilized to much higher pressure in the alloy, with both H_2Se and $(H_2Se)_2H_2$ decomposing above pressures of 23 GPa.[7] Experimentally, we see evidence for an insulator-to-metal transition in phase III at 50 GPa, with band structure calculations showing the static $Cccm$ structure to be metallic (Fig. S15). This occurs concomitantly when the H-bond becomes symmetric and the transition pressure

is dependent on composition, with higher values for increasing sulfur content, demonstrating the ability to tune the electronic properties by varying the S/Se concentration. It would be of great interest to test if the newly synthesised alloy would form an H_3S analogue with superconductive properties, and at what pressure-temperature conditions this would occur.

Table 1: Molecular motions in the structure revealed by Raman and DFT-MD. There are two hydrogen channels, a larger one where the surrounding squares of Se,S are H-bonded, which accommodates the xy-rotor and a narrower one where there are no intermediate hydrogens, and the H_2 molecules point along the channel. The static symmetry labels are obtained by having 3D rotating molecules point along z, thus preserving the symmetry.

Phase	DFT	H_2(S,Se)	H_2 (1)	H_2 (2)	symmetry
I	5GPa	rotating	rotating	rotating	I4/mcm
II	20GPa	H-bond network	rotating	rotating	distorted I4/mcm (I422, P1)
III	60GPa	H-symmetrised	xy-rotor	z-libron	Cccm-type
IV	110GPa	dissociated	dissociated	dissociated	$Im\bar{3}m$-derived

Acknowledgement

Parts of this research were carried out at P02.2 at DESY, a member of the Helmholtz Association (HGF) and we thank H.-P. Liermann and K. Glazyrin for assistance. Parts of this research were carried out at SPring8 and we thank S. Kawaguchi for assistance. The research leading to this result has been supported by the project CALIPSOplus under the Grant Agreement 730872 from the EU Framework Programme for Research and Innovation HORIZON 2020. MPA, GJA, EG and MM acknowledge the support of the European Research Council (ERC) Grant Hecate Ref. No. 695527. Parts of this work was performed under Proposal No. 2017A1062 at SPring-8 and the UKCP collaboration EPSRC grant PO22561. MPA acknowledges UKRI Future Leaders Fellowship Mrc-Mr/T043733/1. R.T.H. would like to acknowledge the support of the National Science Foundation of China (Grant No. 11974034) and ERC Grant "MetElOne" reference No. 948895.

References

(1) Drozdov, A.; Eremets, M.; Troyan, I.; Ksenofontov, V.; Shylin, S. I. Conventional superconductivity at 203 kelvin at high pressures in the sulfur hydride system. *Nature* **2015**, *525*, 73–76.

(2) Duan, D.; Liu, Y.; Tian, F.; Li, D.; Huang, X.; Zhao, Z.; Yu, H.; Liu, B.; Tian, W.; Cui, T. Pressure-induced metallization of dense (H 2 S) 2 H 2 with high-T c superconductivity. *Scientific reports* **2014**, *4*, 6968.

(3) Guigue, B.; Marizy, A.; Loubeyre, P. Direct synthesis of pure H 3 S from S and H elements: No evidence of the cubic superconducting phase up to 160 GPa. *Physical Review B* **2017**, *95*, 020104.

(4) Strobel, T. A.; Ganesh, P.; Somayazulu, M. S.; Kent, P. R.; Hemley, R. Cooperative interactions and novel structural ordering in H2S-H2. *Physical Review Letters* **2011**, *107*.

(5) Pace, E. J.; Liu, X.-D.; Dalladay-Simpson, P.; Binns, J.; Peña-Alvarez, M.; Attfield, J. P.; Howie, R. T.; Gregoryanz, E. Properties and phase diagram of (H 2 S) 2 H 2. *Physical Review B* **2020**, *101*, 174511.

(6) Zhong, X.; Wang, H.; Zhang, J.; Liu, H.; Zhang, S.; Song, H.-F.; Yang, G.; Zhang, L.; Ma, Y. Tellurium hydrides at high pressures: High-temperature superconductors. *Physical Review Letters* **2016**, *116*, 057002.

(7) Pace, E. J.; Binns, J.; Peña Alvarez, M.; Dalladay-Simpson, P.; Gregoryanz, E.; Howie, R. T. Synthesis and stability of hydrogen selenide compounds at high pressure. *The Journal of Chemical Physics* **2017**, *147*, 184303.

(8) Zhang, X.; Xu, W.; Wang, Y.; Jiang, S.; Gorelli, F. A.; Greenberg, E.;

Prakapenka, V. B.; Goncharov, A. F. Synthesis and properties of selenium trihydride at high pressures. *Physical Review B* **2018**, *97*, 064107.

(9) Ren, X.; Ma, Q.; Fan, H.; Pang, L.; Zhang, Y.; Yao, Y.; Ren, X.; Liu, S. F. A Se-doped MoS 2 nanosheet for improved hydrogen evolution reaction. *Chemical Communications* **2015**, *51*, 15997–16000.

(10) Zhang, Y.; Tao, H.; Du, S.; Yang, X. Conversion of MoS2 to a Ternary MoS2–x Se x Alloy for High-Performance Sodium-Ion Batteries. *ACS applied materials & interfaces* **2019**, *11*, 11327–11337.

(11) Zhu, T.; Ding, J.; Shao, Q.; Qian, Y.; Huang, X. P, Se-Codoped MoS2 Nanosheets as Accelerated Electrocatalysts for Hydrogen Evolution. *ChemCatChem* **2019**, *11*, 689–692.

(12) Heil, C.; Boeri, L. Influence of bonding on superconductivity in high-pressure hydrides. *Physical Review B* **2015**, *92*, 060508.

(13) Liu, B.; Cui, W.; Shi, J.; Zhu, L.; Chen, J.; Lin, S.; Su, R.; Ma, J.; Yang, K.; Xu, M., et al. Effect of covalent bonding on the superconducting critical temperature of the HS-Se system. *Physical Review B* **2018**, *98*, 174101.

(14) Amsler, M. Thermodynamics and superconductivity of S x Se 1- x H 3. *Physical Review B* **2019**, *99*, 060102.

(15) van de Walle, A.; Ceder, G. Automating First-Principles Phase Diagram Calculations. *J. Phase Equilib.* **2002**, *23*, 348–359.

(16) Kresse, G.; Furthmuller, J. . *Physical Review B* **1996**, *54*, 11169.

(17) Li, Y.; Wang, L.; Liu, H.; Zhang, Y.; Hao, J.; Pickard, C. J.; Nelson, J. R.; Needs, R. J.; Li, W.; Huang, Y.; Errea, I.; Calandra, M.; Mauri, F.; Ma, Y. Dissociation products and structures of solid H_2S at strong compression. *Physical Review B* **2016**, *93*, 020103.

(18) Ackland, G. Magnetically induced immiscibility in the Ising model of FeCr stainless steel. *Physical review letters* **2006**, *97*, 015502.

(19) Ehteshami, H.; Ackland, G. J. Phase diagram of the frustrated FCC antiferromagnet from effective-field theory. *Journal of Physics: Condensed Matter* **2020**, *32*, 385402.

(20) Goncharov, A. F.; Lobanov, S. S.; Kruglov, I.; Zhao, X.-M.; Chen, X.-J.; Oganov, A. R.; Konôpková, Z.; Prakapenka, V. B. Hydrogen sulfide at high pressure: Change in stoichiometry. *Physical Review B* **2016**, *93*, 174105.

(21) Duwal, S.; Yoo, C.-S. Reversible photochemical transformation of S and H2 mixture to (H2S) 2H2 at high pressures. *The Journal of Physical Chemistry C* **2017**, *121*, 12863–12870.

Graphical TOC Entry